Materials Chemistry and Physics 208 (2018) 169–176

Contents lists available at ScienceDirect

Materials Chemistry and Physics

journal homepage: www.elsevier.com/locate/matchemphys

An insight into formation mechanism of rapid chemical Co-precipitation for synthesizing yttrium iron garnet nano powders

Junliang Liu [a, *], Qimei Jin [a], Shengyun Wang [a], Ping Yu [a], Chong Zhang [a], Clark Luckhardt [b], Zijuan Su [b], Radhika Barua [b], Vincent G. Harris [b]

[a] School of Chemistry and Chemical Engineering, Yangzhou University, Yangzhou 225002, China
[b] Center for Microwave Magnetic Materials and Integrated Circuits, Department of Electrical and Computer Engineering, Northeastern University, Boston, MA 02115, USA

HIGHLIGHTS

- The elements homogeneity in precursor determines the phase evolution process.
- Synthesis temperature decreases if tetragonal YIG exists as the intermediate phase.
- A stable technique is for synthesizing high quality cubic YIG nano powders.

GRAPHICAL ABSTRACT

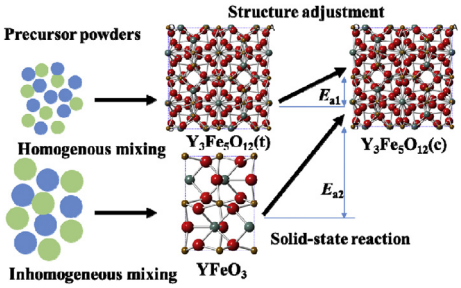

ARTICLE INFO

Article history:
Received 13 September 2017
Received in revised form
5 December 2017
Accepted 9 January 2018
Available online 12 January 2018

Keywords:
Yttrium iron garnet
Nanopowders
Chemical co-precipitation
Phase formation

ABSTRACT

The rapid chemical co-precipitation method is supposed to be a stable way to synthesize high quality cubic yttrium iron garnet (YIG) nanopowders. In this paper, focusing on clarifying its formation mechanism, the thermal behaviors and the elemental distributions of the chemical co-precipitated precursors have been analyzed by simultaneous differential scanning calorimetry plus thermal gravimetric analysis (DSC-TGA) and energy disperse spectroscopy (EDS) mapping technique on a transmission electronic microscope. The results indicated that the homogeneity of Y and Fe elemental distributions in the precursor powders determines the process through which the cubic YIG phase would form: one experiences the intermediate tetragonal YIG phase; the other takes $YFeO_3$ as the intermediate phase. The homogenous distributions of Y and Fe elements in the precursor powders at the scale below 50 nm forms the intermediate tetragonal YIG phase rather than $YFeO_3$, which leads to reduction of the formation temperature for synthesizing the single phase YIG. The obtained YIG nanopowders with the average particle size below 100 nm show excellent magnetic properties with saturation magnetization of 26 emu/g and coercive field of 45 Oe. This clear formation mechanism of YIG nanopowders is suitable for optimizing the processing conditions for the chemical precipitation synthesis of YIG nanopowders at large scale.

1. Introduction

Conventionally, yttrium iron garnet (YIG) with chemical formulation of $Y_3Fe_5O_{12}$ is considered to be an important soft

* Corresponding author.
E-mail address: liujunliang@yzu.edu.cn (J. Liu).

https://doi.org/10.1016/j.matchemphys.2018.01.030
0254-0584/

ferrimagnetic material [1]. It has been widely used in tunable microwave devices due to its superior magnetic properties such as controllable saturation magnetization, low dielectric loss, and narrow ferromagnetic resonance line-width in the microwave region [2]. In the past few years, it has been realized that magnetic nanostructures have superior features owing to their low-dimensional scale effect [3]. Therefore, pure or doped YIG nanomaterials have attracted increasing attention, especially in fields such as Faraday magneto-optical devices for telecommunications [4,5], low temperature co-fired ceramics for microwave integrated circuits [6], exchange coupling nano-magnetisms [7], high-density magnetic or magneto-optical information storage [8], and biomedical hyperthermia [9].

To satisfy the requirements of such applications, high quality YIG nanopowders with precisely designed chemical compositions or specific nanostructures are required [10,11]. Several chemical techniques including the hydrothermal approach [12], chemical coprecipitation route [13], sol-gel auto-combustion technique [14], and micro-emulsion method [15] were developed to fabricate YIG-related nanomaterials. Among them, chemical coprecipitation method is considered suitable for mass production as it is a relatively low-cost technique [16,17]. It has been extensively used to fabricate pure or doped YIG nanopowders [13,18–23]. However, its obstacle is the high secondary sintering temperature, as high as 1100 °C, which leads to coarsening of the synthesized nanoparticles. To decrease the secondary sintering temperature, the co-precipitates as the precursors for heating treatment should be simultaneously generated and homogenously mixed during the chemical co-precipitating reaction, which is believed to be a decisive factor governing the formation of crystalline phases during the calcination of co-precipitates [21]. Focusing on this, many studies have been performed to refine the chemical co-precipitation technique using various kinds and amounts of precipitators, employing surfactants in the co-precipitation process, and optimizing the sintering temperature. YIG spherical particles were successfully synthesized via co-precipitation using nitrates or chlorides as the starting materials, urea or ammonia solution as the precipitant, and PVP and ammonium iron (III) sulfate as the surfactants. The formation of crystalline phases from the precipitate was found to start at 800 °C and yield an orthorhombic YIG phase up to 1000 °C. After further calcination at 1100 °C, a single cubic phase YIG was obtained and the powder particles were of an average size of ~0.5 μm [18]. When using NaOH solution as the precipitating agent, single-phase YIG powders can be obtained only after calcining the precipitates at 1200 °C [19]. Altering the mixing sequence by adding the solution of metal salts into the precipitant solution instead of precipitant into the salts solution, it was found that the target YIG phase was more easily formed at about 1000–1100 °C [20]. It indicated that the target YIG phase was formed more easily if reverse strike co-precipitation was used. Considering this, and based on experimental designs, Zhang, et al. improved the chemical co-precipitation method by rapidly pouring a solution of nitrates into a large amount of ammonia solution (1:4). The results indicated that there was no $YFeO_3$ in the emerging intermediate phase and single phase YIG nanopowders could be synthesized at a temperature as low as 750 °C [13]. Such a method provides a stable technique to synthesize high quality YIG nanopowders several tens of nanometers in size. However, why was there no $YFeO_3$ in the intermediate phase? How can we control the synthesis route to obtain YIG nanopowders with low-temperature secondary sintering in the chemical co-precipitation technique or other soft chemical methods? The formation mechanism is very important but still not very clear. Therefore, to clarify this, the thermal behaviors and elemental distributions in the precursor powders are extremely important. In this paper, the possible formation mechanism for the rapid chemical co-precipitation method has been conceived based on the systematical investigation on influence of the precipitating agent solution. sintering temperature on the phase formation and particle morphology. Moreover, the relationships of the magnetic properties with microstructures of the synthesized powders have been discussed.

2. Material and methods

The rapid chemical co-precipitation technique plus secondary heating treatment was used to synthesize YIG nanopowders, which is similar to the method firstly reported by Zhang et al. [13] and briefly described as follows: yttrium nitrate hexahydrate and ferric nitrate nonahydrate were used as the starting materials, weighed according to the stoichiometric ratio and dissolved in deionized water to form an aqueous solution of nitrates. The concentrations of yttrium nitrate and ferric nitrate solution were 0.625 mol/L and 0.375 mol/L, respectively. Ammonia solution with a concentration of 28 wt% was chosen as the precipitator with various ratios of starting solution to ammonia solution (S/A). Under vigorous stirring, the starting solution was poured into the ammonia solution and allowed to react for about an hour. Subsequently, the as-formed precipitates were collected from the solution by vacuum filtration and washed with ethanol twice before moderate drying at 60 °C for 12 h. The dried precipitates were slightly ground into precursor powders and placed in a furnace for thermal treatment at different temperatures ranging from 650 to 900 °C for 2 h with a temperature ramping rate of 5 °C/min.

The infrared spectrums of the precipitates and synthesized powders were collected (FT-IR, Varian 670) was utilized with KBr disc method the range of 4000 to 400 cm^{-1}. The phase compositions and crystal structures of the synthesized powders were identified using X-ray diffraction (XRD). The measurement was carried out on a Rigaku Ultima III using a Cu-K_α radiation source. The elemental distribution in the precursor precipitate was identified using energy disperse spectroscopy (EDS) mapping technique on a transmission electronic microscope (TEM, FEI Tecnai G2 F30 S-TWIN) and their thermal behavior was recorded by simultaneous differential scanning calorimetry plus thermal gravimetric analysis (DSC-TGA, TA, SDT Q600). The particle size and morphology were observed using TEM (Philips, Tecnai 12). The magnetic properties were measured with a vibrating sample magnetometer (VSM, Lakeshore 7400).

3. Results and discussion

The FT-IR spectrums of the precipitates and synthesized powders at various temperatures were collected and shown in Fig. 1. The absorption bands around 3418 cm^{-1}, 1640 cm^{-1}, 1504 cm^{-1}, and 1381 cm^{-1}, assigned to O-H bonds, absorbed water molecules, NH_4^+ radicals, and NO_3^-radicals, vanished as the firing temperature achieved to 750 °C, indicating the complete elimination of water and decomposition of precursors. As the firing temperature was over 750 °C, the new week absorption bands at 561, 594 and 662 cm^{-1} represented the formation of YIG phase [13]. The increasing intensity of these absorptions referred to increasing crystallinity of YIG.

Fig. 2 demonstrates the XRD patterns of the powders synthesized using the rapid chemical co-precipitation method. Single-phase YIG powders were successfully fabricated with different S/A, indicating that almost all the metal elements were precipitated into the precursor powders and there was little deviation from the element ratio in the YIG phase. There were two differences in the phase evolution of YIG synthesized with different S/A values: 1) as the S/A value decreased, the temperature to form the single phase

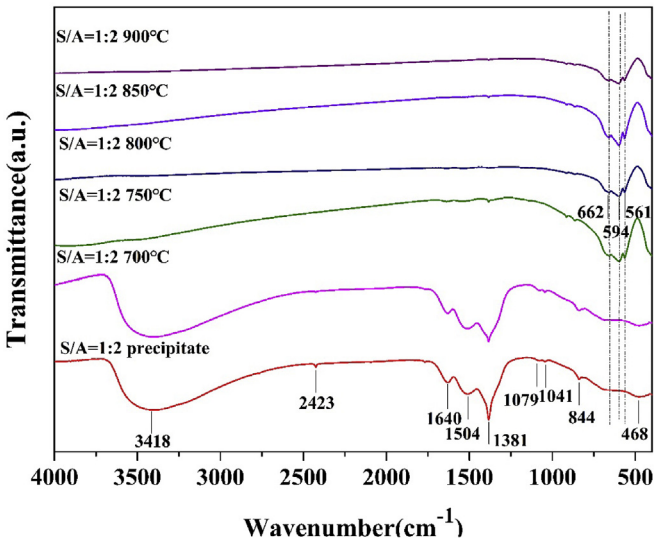

Fig. 1. IR spectrums of the precipitates and synthesized powders at various temperatures with S/A of 1:2.

YIG decreased from 850 °C to 750 °C; and 2) when the S/A value was 1:1, $YFeO_3$ existed as the intermediate phase, which was very difficult to transform to YIG phase. As the S/A value changed to 1:2 and 1:4, tetragonal YIG was the intermediate phase formed instead of $YFeO_3$.

Why were there such great differences? What controls this phase evolution process? To answer these two questions, attention should be paid to two things: 1) the elemental contents and distributions in the precursor powders, and 2) the thermal behavior of the precursor powders.

First, the EDS mapping technique was employed to confirm the elemental contents in the precursor powders and to analyze the element distribution. The Y and Fe elemental contents were very similar to that in the starting materials according to the formula of YIG. This agrees with the observation from the XRD patterns that all the precursor powders were transformed into single-phase YIG powders. However, there were obvious distinctions in the Y and Fe elemental distributions in the different precursor powders, as shown in Fig. 3. From the elemental distribution map with different characteristic absorptions, it was easy to find that the Y distribution was different from the Fe element distribution at the 50 nm scale when S/A was 1:1. They were of different shapes, indicating Y-enrichment in micro-domains. When S/A was 1:2 or 1:4, both Fe and Y elemental distributions were of similar shapes, confirming the homogenous mixing of Fe and Y in the precursor powders at the scale below 50 nm. Increasing the amount of precipitating agent poured into the starting metal salts solution increased the rapidity with which the chemical co-precipitation reaction took place, resulting in smaller precipitate particles and improved homogeneity of the metal elements [13,22].

The difference in homogeneity of the metal elements affected thermal decomposition and solid-state reactions, which could be identified by thermal analysis. Fig. 4 gives the TG-DSC curves of the precursor powders with different S/A values. The endothermic peaks below 100 °C with a weight loss less than 9 wt% resulted from the evaporation of the residual solvents like ethanol and water. When the S/A was 1:1, the TG curve showed a weight loss of about 25 wt% in a wide temperature range from 100 °C to about 770 °C. This should be ascribed to the decomposition of amorphous precipitates into oxides [23]. However, a similar loss in weight took place in a relatively narrow range from 100 °C to about 500 °C as

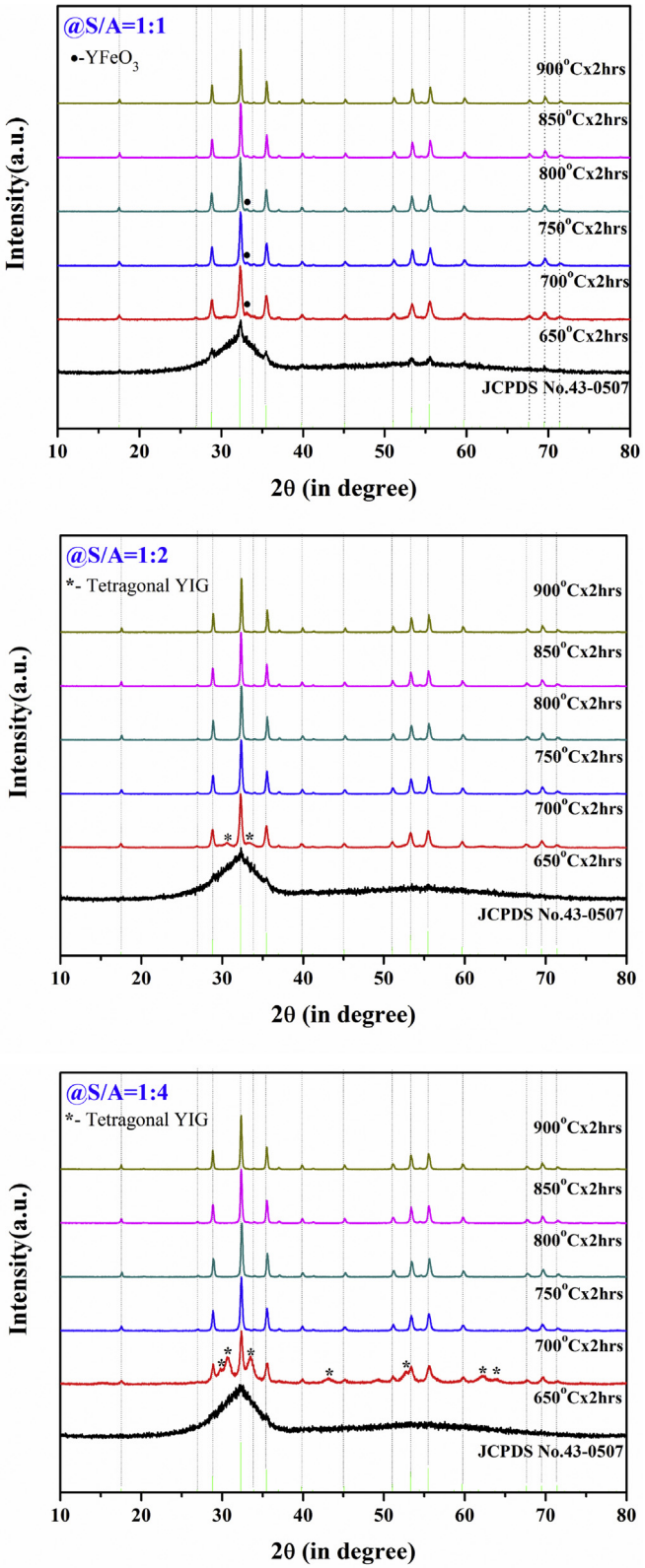

Fig. 2. XRD patterns of the powders synthesized by the rapid chemical co-precipitation plus secondary heating treatment at various temperatures for 2 h.

the S/A decreased to 1:2 or 1:4. This indicated that the precursor powders were conducive to accomplishing the decomposition process. All the DSC curves demonstrated a diffused exothermic

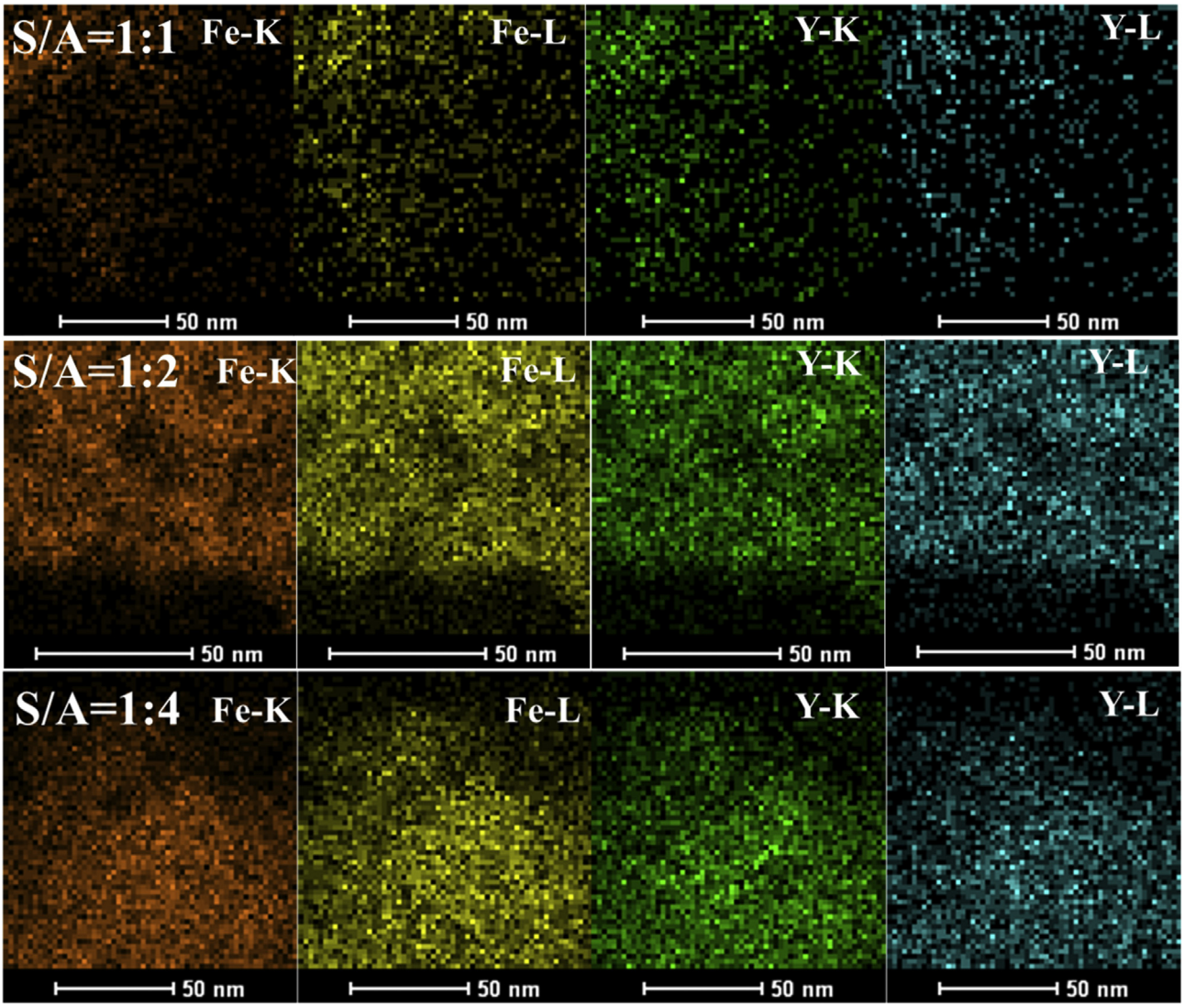

Fig. 3. EDS mapping images of yttrium and iron element distribution in precursor powders.

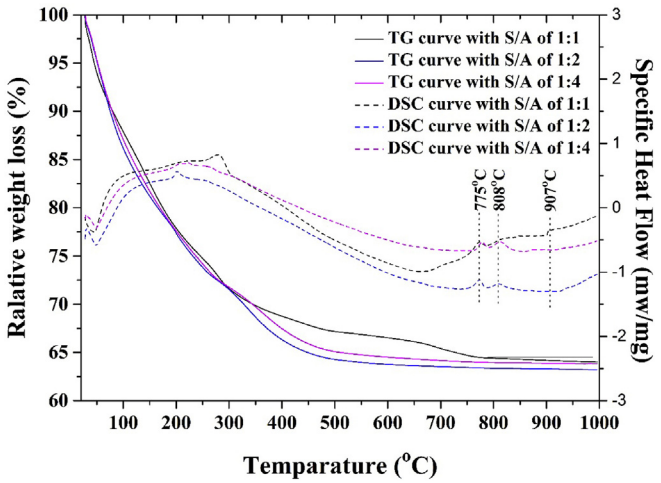

Fig. 4. TG-DSC curves of the precursor powders with different S/A values.

peak at a similar temperature of about 775 °C. This peak characterized by low weight loss should be attributed to the formation of orderly complex oxides by solid-state reaction of the decomposition product of the precursors. However, at a different S/A value, another exothermic peak at a higher temperature appeared to be very different. The peak position was about 907 °C as S/A was 1:1, which was about 100 °C, higher than those when S/A was 1:2 or 1:4. Obviously, there must be different phase evolution processes with different S/A values. This agreed with the results from the XRD patterns. Moreover, the precursor powders could transform to the single-phase YIG powders more easily when S/A was 1:2 or 1:4 than when it was 1:1 owing to the homogenous elemental distribution in the precursor powders.

Based on the analysis from XRD, EDS mapping, and TG-DSC results, there are two routes for the formation of YIG from amorphous precipitates as follows:

Route-1: Fe-precipitate + Y-precipitate → $5Fe_2O_3+3Y_2O_3 \rightarrow 2Fe_2O_3+6YFeO_3 \rightarrow 2Y_3Fe_5O_{12}(c)$

Route-2: Fe-precipitate + Y-precipitate → $5Fe_2O_3+3Y_2O_3 \rightarrow 2Y_3Fe_5O_{12}(t) \rightarrow 2Y_3Fe_5O_{12}(c)$

These are also proposed in the reports [13,18–21]. While $YFeO_3$ is the intermediate phase in Route-1, tetragonal $Y_3Fe_5O_{12}$ becomes the intermediate phase in Route-2. Tetragonal and cubic $Y_3Fe_5O_{12}$ have similar crystal structures resulting in easy transformation of the tetragonal to the cubic phase by atomic re-arrangement with a small activation energy. Therefore, the target cubic YIG phase could be formed at a lower temperature. If $YFeO_3$ exists as the intermediate phase, it could transform to the cubic YIG phase with diffusion and reaction. This process must be of higher activation energy requiring higher temperature to form the target YIG phase. From this point of view, it is extremely important to clarify what makes the process take Route-1 or Route-2. As illustrated in Fig. 5, the homogeneity of the Y or Fe elemental distribution in the precursor powders is the factor that determines this. If Y or Fe is mixed homogenously even in the very small domain, Route-2 could be the phase evolution process of the YIG. In our work, the scale of the small domain should be below 50 nm.

After clarifying the phase formation mechanism of YIG using this rapid chemical co-precipitation and secondary heating treatment, we characterized the micro-structural behavior and other characteristics of the synthesized YIG powders. Based on the full width at half maximum (FWHM) of the highest (420) plane reflection, the grain size of the synthesized YIG powders was calculated using the Scherrer formula:

$$D = k\lambda/\beta\cos\theta \quad (1)$$

where k, λ, β, θ are Scherrer parameter, X-ray wavelength, FWHM and Bragg angle in degree, respectively. The calculated crystal size is presented in Fig. 6. The crystal size increased linearly as a function of the secondary heating temperature, but there were different slopes for the different S/A values. Generally, the energy for secondary heating treatment could be divided into two parts: for the diffusion and solid-state reaction to form the targeted phase; and for the particle growth. Since it was relatively difficult to form the single phase YIG when S/A was 1:1, the corresponding crystal size gradually increased at a lower temperature and dramatically

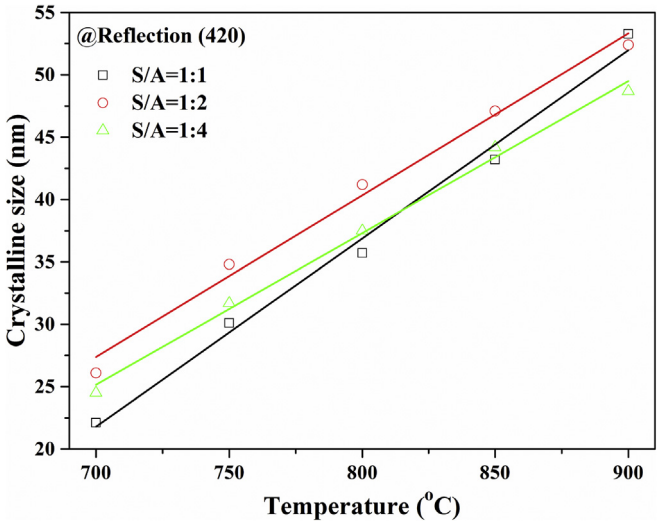

Fig. 6. Calculated crystalline sizes of the synthesized YIG nano powders with various S/A ratios.

increased after forming the targeted phase. Typically, the obtained single-phase YIG powders increased from 26 to 52 nm when the secondary heating temperature was increased from 750 °C to 900 °C when the S/A was 1:2.

Fig. 7 gives the TEM images for the as-synthesized YIG nanopowders with S/A of 1:2 at various heating temperatures. All the powders demonstrated severe agglomeration between small particles due to the high specific surface tension and sintering adhesion. The particles were irregular. Nevertheless, it was easy to find that the particle size increased as the heating temperature went from 750 °C to 900 °C. The average particle size of the synthesized powders at 750 °C was about 60 nm compared to 150 nm at 900 °C. The particle size was much larger than the crystal size calculated from XRD patterns, which revealed that single particles should actually be the result of the agglomeration of several nanocrystals. The selective area diffraction image of the sample synthesized at 800 °C for 2 h with S/A of 1:2 was shown in Fig. 8. From the images,

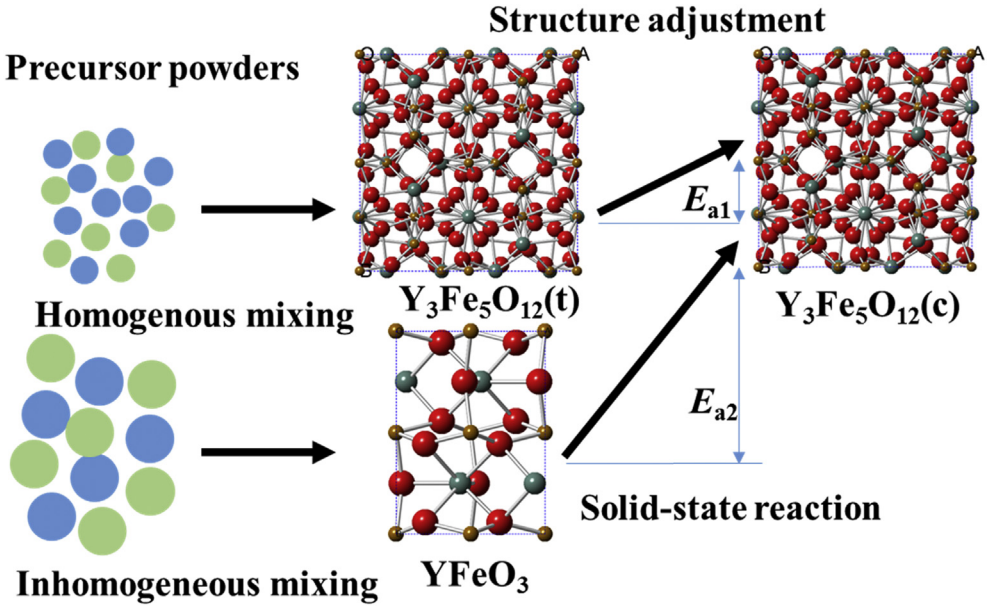

Fig. 5. Illustration of the phase formation mechanism for rapid chemical co-precipitation plus secondary heating treatment.

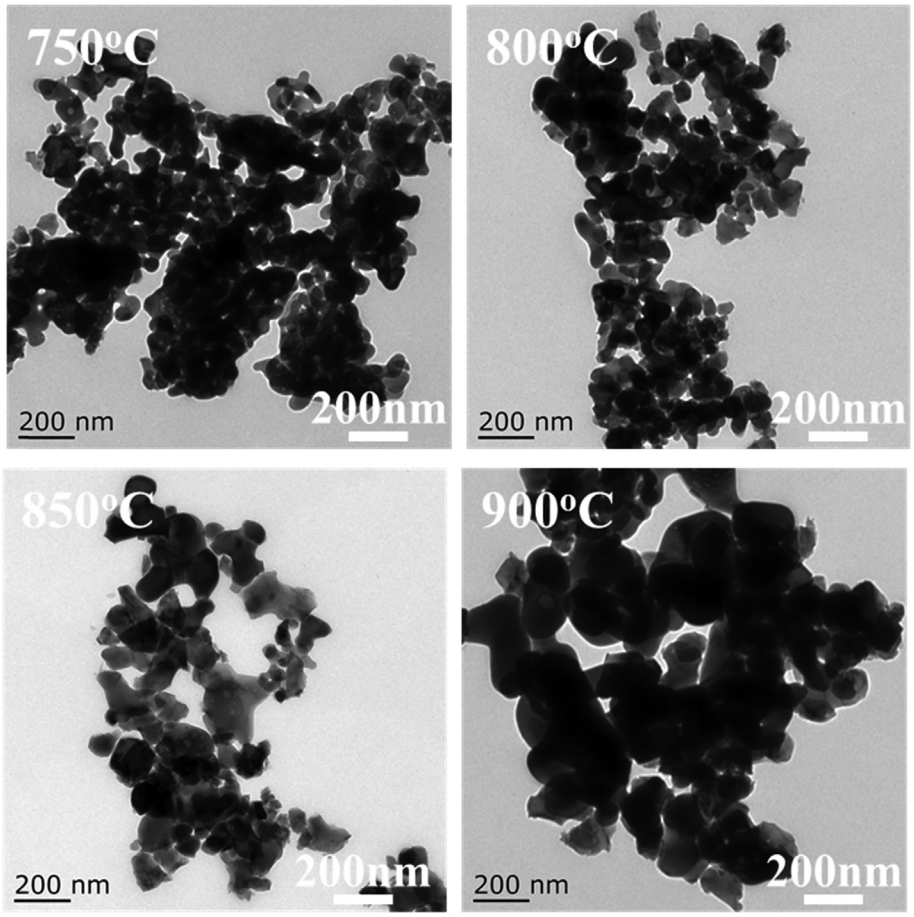

Fig. 7. Typical TEM images of the YIG nano powders synthesized with the S/A of 1:2.

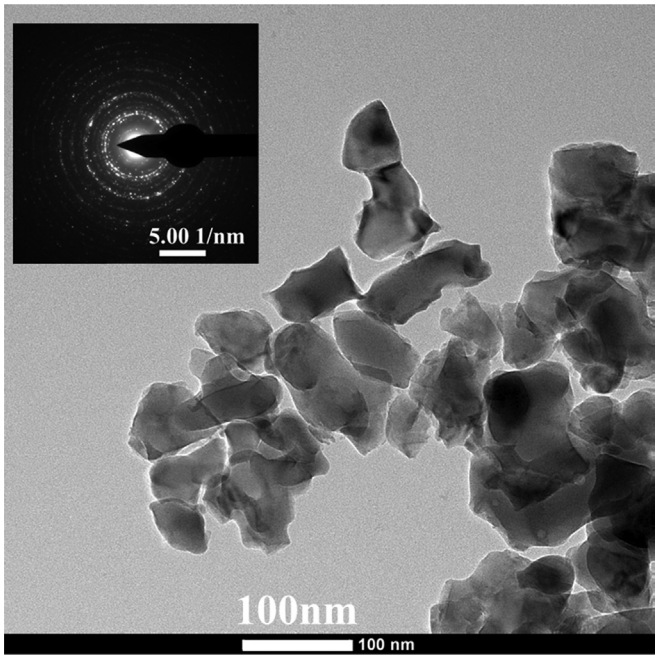

Fig. 8. TEM image and selective area electronic diffraction pattern of the YIG powders synthesized at 800 °C for 2 h with S/A of 1:2.

electronic diffraction pattern demonstrated an inconsecutive ring with lots of diffraction spots, indicating that the particle consists of nano crystals.

The magnetic hysteresis loops of the nanopowders synthesized with various S/A ratios were measured at room temperature as shown in Fig. 9, which demonstrated the easy magnetization behavior of YIG with a small coercive field (H_c). The variation in the saturation magnetization (M_s) was related to the phase compositions and microstructures of the synthesized powders. The corresponding saturation magnetizations and coercive fields are illustrated in Fig. 10. There was a remarkable increase in saturation magnetization with increasing heating temperature due to the initial formation of YIG magnetic powders from the amorphous hydroxide precipitates [13,18,20]. As the temperature increased further from 800 °C to 900 °C, the transformation from partial-disorder of the magnetic moments in the materials to complete-order contributed to the gradual increase in the saturation magnetization. It was noted that the saturation magnetization of all the synthesized single phase YIG nanopowders with different S/A values approached a similar value of ~25 eum/g, which agreed with the report of YIG nanopowders [13,18,20]. The highest value of saturation magnetization was ~26 emu/g when S/A was 1:2 at 900 °C, indicating high purity and good evolution of every grain. The coercive fields for YIG nanopowders linearly increased from about 10 Oe to 45 Oe as the temperature increased from 750 °C to 900 °C. The critical size of YIG single domain particles is about

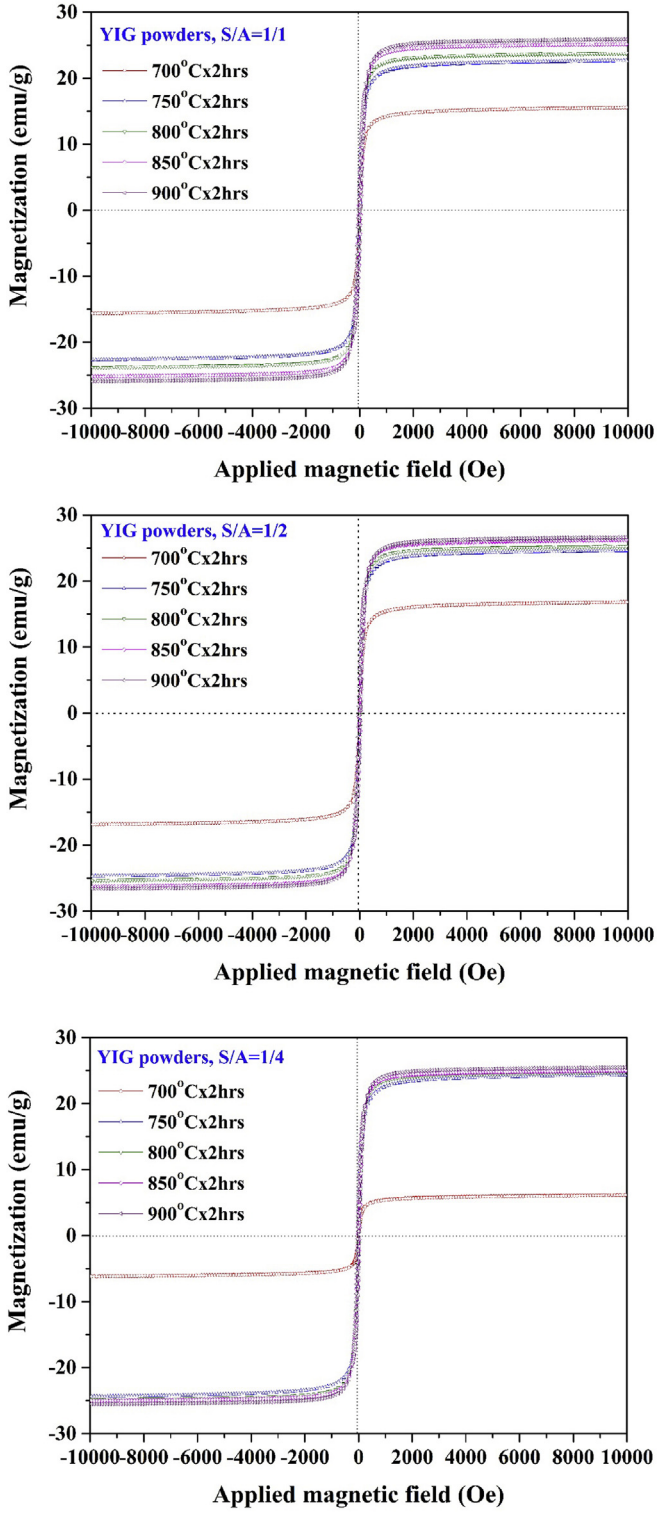

Fig. 9. Magnetic hysteresis loops of the synthesized nano powders with various S/A ratios.

190 nm [24,25] and the particle sizes of the synthesized powders were below 100 nm, a tendency ascribed to a typical particle-size dependence of the coercive field for ferrimagnetic single domain particles [24–26].

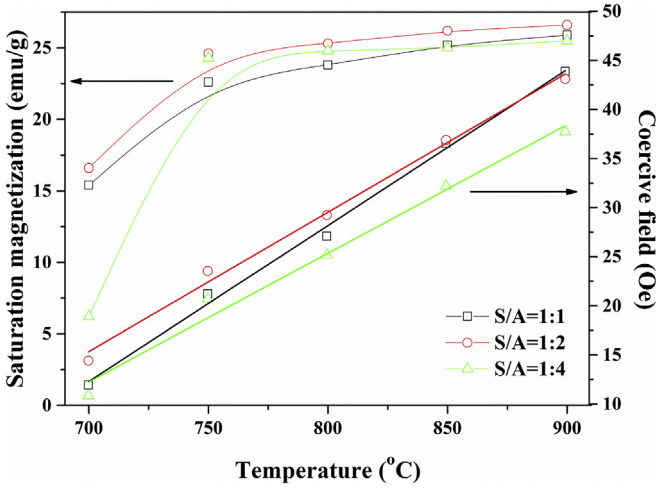

Fig. 10. Magnetic parameters of the synthesized nano powders with various S/A ratios.

4. Conclusions

Single phase YIG nanopowders with particle size below 100 nm were synthesized by the rapid chemical co-precipitation method with secondary heating treatment. The obtained YIG nanopowders show excellent magnetic properties with a saturation magnetization of 26 emu/g and a coercive field of 45 Oe. The homogeneity of Y and Fe in the precursor powders causes formation of the intermediate tetragonal YIG phase instead of $YFeO_3$, which leads to a decrease in the temperature for synthesizing the single phase YIG. This clear formation mechanism of YIG nanopowders is suitable for optimizing the processing conditions for the chemical precipitation synthesis of YIG at large scale.

Acknowledgments

Dr. Junliang Liu acknowledges financial support from the National Natural Science Foundation of China (No.51678292), China Postdoctoral Science Foundation (No. 2016T90512, No. 2015M570483), the Scholarship of Jiangsu Government for Overseas Study, and the Project Funded by the Priority Academic Program Development of Jiangsu Higher Education Institutions (Chemistry).

References

[1] David Jiles, Introduction to Magnetism and Magnetic Materials, third ed., CRC Press-Taylor & Francis Group, United Kingdom, 2016.
[2] Nan Mo, Jerome J. Green, Pavol Krivosik, Carl E. Patton, The low field microwave effective linewidth in polycrystalline ferrites, J. Appl. Phys. 101 (2007), 023914.
[3] Alberto Passos Guimarães, Principles of Nanomagnetism (NanoScience and Technology) 2009th Edition, Springer, 2009.
[4] Toshihiro Shintaku, Takehiko Uno, Morio Kobayashi, Magneto-optic channel waveguides in Ce-substituted yttrium iron garnet, J. Appl. Phys. 74 (1993) 4877–4882.
[5] Dainan Zhang, Lichuan Jin, Huaiwu Zhang, Qinghui Yang, Yiheng Rao, Qiye Wen, Tingchuan Zhou, Cheng Liu, Zhiyong Zhong, John Q. Xiao, Chemical epitaxial growth of nm-thick yttrium iron garnet films with low Gilbert damping, J. Alloy. Compd. 695 (2017) 2301–2305.
[6] Ning Jia, Zhang Huaiwu, Jie Li, Yulong Liao, Lichuan Jin, Cheng Liua, Vincent G. Harris, Polycrystalline Bi substituted YIG ferrite processed via low temperature sintering, J. Alloy. Compd. 695 (2017) 931–936.
[7] Miao Liu, Haibo Yang, Ying Lin, Yanyan Yang, One-step synthesis of homogeneous $BaFe_{12}O_{19}/Y_3Fe_5O_{12}$ composite powders, Mater. Res. Bull. 60 (2014) 195–200.
[8] A.C. Rastogi, V.N. Moorthy, Sandip Dhara, Cobaltous oxide infiltrated yttrium iron garnet thin films as high-coercivity media for data storage, Appl. Phys. Lett. 78 (2001) 1709–1711.

[9] S. Mornet, S. Vasseur, F. Grasset, P. Veverka, G. Goglio, A. Demourgues, J. Portier, E. Pollert, E. Duguet, Magnetic nanoparticle design for medical applications, Prog. Solid State Chem. 34 (2006) 237–247.
[10] Christian Suchomski, Christian Reitz, Celia T. Sousa, Joao P. Araujo, Torsten Brezesinski, Room temperature magnetic rare-earth iron garnet thin films with ordered mesoporous structure, Chem. Mater. 25 (2013) 2527–2537.
[11] A. Jalalian, M.S. Kavrik, S.I. Khartsev, A.M. Grishin, Ferromagnetic resonance in $Y_3Fe_5O_{12}$ nanofibers, Appl. Phys. Lett. 99 (2011) 102501.
[12] Yong S. Cho, Vernon L. Burdick, Vasantha R.W. Amarakoon, D. Kuse, C. Schüler, A. Beck, Hydrothermal preparation and morphology characteristics of $Y_3Fe_5O_{12}$, J. Am. Ceram. Soc. 80 (1997) 1605–1608.
[13] Zhang Wei, Guo Cuijing, Ji Rongjin, Fang Caixiang, Zeng Yanwei, Low-temperature synthesis and microstructure-property study of single-phase yttrium iron garnet (YIG) nanocrystals via a rapid chemical coprecipitation, Mater. Chem. Phys. 125 (2011) 646–651.
[14] S. Hosseini Vajargah, H.R. Madaah Hosseini, Z.A. Nemati, Preparation and characterization of yttrium iron garnet (YIG) nanocrystalline powders by auto-combustion of nitrate-citrate gel, J. Alloy. Compd 430 (2007) 339–343.
[15] Vaqueiro Paz, Lpez-quintela M. Arturo, Rivas Jos, Synthesis of yttrium iron garnet nanoparticles via coprecipitation in microemulsion, J. Mater. Chem. 7 (1997) 501–504.
[16] Liu Junliang, Liu Ping, Zhang Xingkai, Pan Dongjun, Zhang Peng, Zhang Ming, Synthesis and properties of single domain sphere-shaped barium hexa-ferrite nano powders via an ultrasonic-assisted co-precipitation route, Ultrason. Sonochem. 23 (2015) 46–52.
[17] Junliang Liu, Xiulei Chen, Leiming Yan, Shengyun Wang, Ming Zhang, Synthesis and properties of single domain strontium hexa-ferrite ultrafine powders via a surfactant-assisted Co-precipitation method, J. Electron. Mater. 44 (2015) 2276–2282.
[18] M. Jafelicci Jr., R.H.M. Godoi, Preparation and characterization of spherical yttrium iron garnet via coprecipitation, J. Magn. Magn Mater. 226–230 (2001) 1421–1423.
[19] M.M. Rashad, M.M. Hessien, A. Ei-Midany, I.A. Ibrahim, Effect of synthesis conditions on the preparation of YIG powders via coprecipitation method, J. Magn. Magn Mater. 321 (2009) 3752–3757.
[20] L. Fernandez-Garcia, M. Suarez, J.L. Menendez, Synthesis of mono and multidomain YIG particles by chemical coprecipitation or ceramic procedure, J. Alloy. Compd 495 (2010) 196–199.
[21] M. Ristic, I. Nowikb, S. Popovic, I. Felner, S. Music, Influence of synthesis procedure on the YIG formation, Mater. Lett. 57 (2003) 2584–2590.
[22] Botao Huang, Rui Ren, Zhao Zhang, Shuping Zheng, The improvement of dispersibility of YIG precursor prepared via chemical coprecipitation, J. Alloy. Compd 558 (2013) 56–61.
[23] Yen-Pei Fu, Feng-Yi Tsai, Nonisothermal crystallization kinetics of $Bi_xY_{3-x}Fe_5O_{12}$ ($0.25 \leq x \leq 1.00$) prepared from coprecipitation process, J. Am. Ceram. Soc. 91 (2008) 1214–1217.
[24] R.D. Sánchez, J. Rivas, P. Vaqueiro, M.A. López-Quintela, D. Caeiro, Particle size effects on magnetic properties of yttrium iron garnets prepared by a sol-gel method, J. Magn. Magn Mater. 247 (2002) 92–98.
[25] P. Vaqueiro, M.A. López-Quintela, J. Rivas, J.M. Greneche, Annealing dependence of magnetic properties in nanostructured particles of yttrium iron garnet prepared by citrate gel process, J. Magn. Magn Mater. 169 (1997) 56–58.
[26] Rodziah Nazlan, Mansor Hashim, Idza Riati Ibrahim, Dependence of magnetic hysteresis on evolving single-sample sintering in fine-grained yttrium iron garnet, J. Supercond. Nov. Magn 27 (2014) 631–639.